PROTEINS: Structure, Function, and Genetics 8:377–385 (1990)

Refinement of the NMR Structures for Acyl Carrier Protein With Scalar Coupling Data

Yangmee Kim and James H. Prestegard
Department of Chemistry, Yale University, New Haven, Connecticut 06511

ABSTRACT **Structure determination of small proteins using NMR data is most commonly pursued by combining NOE derived distance constraints with inherent constraints based on chemical bonding. Ideally, one would make use of a variety of experimental observations, not just distance constraints. Here, coupling constant constraints have been added to molecular mechanics and molecular dynamics protocols for structure determination in the form of a psuedoenergy function that is minimized in a search for an optimum molecular conformation. Application is made to refinement of a structure for a 77 amino acid protein involved in fatty acid synthesis, *Escherichia coli* acyl carrier protein (ACP). 54 $^3J_{HN\alpha}$ coupling constants, 12 coupling constants for stereospecifically assigned side chain protons, and 450 NOE distance contraints were used to calculate the 3-D structure of ACP. A three-step protocol for a molecular dynamics calculation is described, in analogy to the protocol previously used in molecular mechanics calculations. The structures calculated with the molecular mechanics approach and the molecular dynamics approach using a rigid model for the protein show similar molecular energies and similar agreement with experimental distance and coupling constant constraints. The molecular dynamics approach shows some advantage in overcoming local minimum problems, but only when a two-state averaging model for the protein was used, did molecular energies drop significantly.**

Key words: structure determination, two-dimensional NMR, molecular mechanics, molecular dynamics, conformational equilibrium

INTRODUCTION

Recently, advances in NMR technology and computational methods have allowed the determination of three-dimensional structures of small proteins in solution.[1–6] Most of these determinations rely primarily on interproton distances measured from 2-D NOESY experiments, and use scalar coupling connectivities from 2-D COSY experiments only for assignment purposes.

In principle, scalar coupling constants can provide important structural information as well as aid in assignment. Experimentally determined three bond coupling constants can be converted into dihedral angles using Karplus type relationships.[7–9] These dihedral angles, particularly along a peptide backbone, can provide a wealth of structural information on proteins. Some proof of this utility lies in the frequent use of ranges of dihedral angles found in known X-ray structures to impose constraints on backbone structures of unknown proteins.[10–14] Actual measurement of coupling constants in the protein of interest could make constraints more stringent and greatly improve the structures.

Measurement and interpretation of coupling constants in terms of dihedral angles are unfortunately not straightforward. Direct measurement of coupling constants in coupling correlated 2D NMR experiments provides unrealistically large values because of cancellation of antiphase components of cross-peaks.[15] This has resulted in the need for very time-consuming simulation of spectra or use of approximate couplings.[16,17] Interpretation is also complicated by the fact that a coupling constant can correspond to more than one dihedral angle, and the fact that the coupling constant may be the result of motional averaging. These problems must be addressed in any analysis procedure.

Recently, we developed a simple method which allows accurate calculation of scalar couplings from measurement of separations of extrema in dispersive and absorptive plots of rows through COSY cross peaks.[18] Use of this new information in conjunction with NOE constraints and the empirical molecular force field of a widely used modeling pack-

Received November 29, 1989; revision accepted May 11, 1990.

Address reprint requests to Dr. James H. Prestegard, Department of Chemistry, Yale University, New Haven, CT 06511.

Abbreviations: 2-D NOSEY, two-dimensional nuclear Overhauser enhancement and exchange spectroscopy; 2-D COSY, two-dimensional coupling correlated spectroscopy; E.COSY, exclusive COSY; P.E.COSY, primitive E.COSY; DQF-COSY, double-quantum filtered COSY; ACP, acyl carrier protein; TPPI, time proportional phase incrementation; AMBER, assisted model building with energy refinement; DISGEO, distance geometry; NOE, nuclear Overhauser effect.

age is presented here. A new pseudoenergy term, which is a function of experimental coupling constants, is introduced. To address the problem of multiple minima in this function, both molecular mechanics and molecular dynamics calculations are performed and compared. For the case in which the observed coupling constant is the result of motional averaging, a two-state model is presented. *Escherichia coli* acyl acrrier protein (ACP), an important cofactor in fatty acid synthesis, provides a suitable test subject for these new protocols. Structures for ACP have been derived previously using NOE distance constraints[4,14,19] and evidence has been presented showing that conformational averaging effects may exist.

MATERIALS AND METHODS

Three bond amide to α proton coupling constants, $^3J_{HN\alpha}$, for ACP were calculated as described previously.[18] A DQF-COSY data set,[20] previously acquired on a Bruker AM 500 spectrometer was zero-filled to 4K × 2K, giving a digital resolution of 1.2 Hz/pt in F_2 and processed with an exponential weighting function (line broadening equal to 1 Hz) in t_2. The peak-to-peak separation of outer extrema in dispersive and absorptive spectra were measured and converted into J coupling constants.

In order to measure accurate $^3J_{\alpha\beta}$ coupling constants for ACP, a new P.E.COSY[21,22] spectrum was acquired on a 490 MHz home-built spectrometer. The ACP was isolated and purified as described in the literature[23] and prepared as a 7 mM sample in 55 mM KH_2PO_4-D_2O at pH 5.9. Using a small flip angle for the final pulse in a COSY experiment, 39°, a spectrum very similar to an E.COSY spectrum[24,25] is obtained. In P.E.COSY and E.COSY, the components of the 2-D cross-peaks arising from passive spin–spin couplings are either eliminated or significantly reduced in intensity.[21,22,24,25] This leads to less severe overlap within the multiplets and allows for more accurate determination of ^3J passive coupling constant values by direct measurement. Data were recorded in phase-sensitive mode by TPPI,[26,27] and processed on a Vax 3200 computer with the FTNMR software program.[28] The data set was zero-filled to 4K, giving a digital resolution of 1.1 Hz/pt in F_2, and multiplied in both dimension by a sine-bell function phase shifted by 8°.

Measured coupling constants are incorporated into a molecular structure search strategy by defining a suitable pseudoenergy function. Ideally this function should employ conformation variables compatible with those employed in a molecular force field. In analogy with the pseudoenergy function used previously for proton–proton internuclear distance constraints, it should also be an appropriate error function which minimizes when suitable conformations are found.[29]

There are well-defined relationships between dihedral angles and scalar couplings of vicinally bonded protons.[7–9] We used the modified Karplus equation for $^3J_{HN\alpha}$ shown in Eq. (1) to rewrite measured couplings in terms of vicinal proton dihedral angles, Θ.[10]

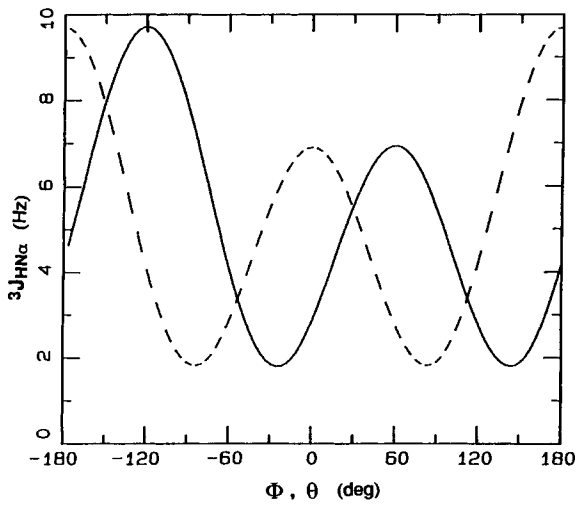

Fig. 1. Relationship between the vicinal coupling constant $^3J_{HN\alpha}$ and angles Θ and Φ. Angular dependence of J on Φ is shown with solid lines and angular dependence of J on Θ is shown with dotted lines. Angle Θ is the value Θ = | Φ−60°|.

$$^3J_{HN\alpha} = 6.4 \cos^2 \Theta - 1.4 \cos \Theta + 1.9 \quad (1)$$

Because in our force field covalent geometry is pretty soft and variations in Φ more directly influence the backbone conformation during energy minimization, the backbone torsion angle, Φ, proves to be more useful than the angle Θ. Equation (1) can be recast in terms of Φ.

$$^3J_{HN\alpha} = -3.2 \cos^2 \Phi + 2.8 \sin 2\Phi - 0.7 \cos \Phi - 1.2 \sin \Phi + 6.7 \quad (2)$$

Figure 1 shows the relationship between $^3J_{HN\alpha}$, Θ, and Φ.[10] It has become common practice to constrain Φ, the backbone torsion angle, to some specific range of torsion angles based on an estimated $^3J_{HN\alpha}$ or on the basis of most probable angles from X-ray structures.[10–14] This is often done with a modified square well having bounds set at upper and lower limits for Φ.[30,31] As shown in Figure 1, from coupling constants alone it is not possible to go uniquely to one value of Φ or one range of Φ values. There can be as many as four possible torsion angle solutions for a given J. Some of these will be excluded by sterically prohibited conformations in the molecular force field. Others will be excluded by NOE distance constraints. Therefore it should not be necessary to refine this function further. We can simply define a pseudoenergy function as follows:

$$E_{\text{pseudo } J} = W (J_c - J_0)^2 \quad (3)$$

Here W is a weighting factor (kcal/mol/Hz^2), J_0 is the directly measured experimental coupling constant and J_c is a term calculated from the internal coordinates of a trial structure using Eq. (2). This energy is added for each measured J along with other pseudoenergy terms to energies normally present in a molecular dynamics and molecular mechanics force field.

For side chains it is also desirable to recast a Karplus relationship[32] in terms of a heavy atom dihedral in order to improve convergence. In cases where a united atom force field can be used this also allows a reduction in numbers of atoms in the calculation. Again the inverted form of this function has multiple solutions in terms of the side chain dihedral χ. The situation is, however, different in that we frequently make two measurements that pertain to the same χ value, one for the β pro R and one for the β pro S proton. In the course of making stereospecific assignments of these protons a specific value for χ is often obtained. Therefore, in this case, we write a pseudoenergy function directly in terms of χ, where W' is a weighting factor in kcal/mol/degree^2

$$E_{\text{pseudo }\chi} = W' (\chi - \chi_0)^2 \quad (4)$$

If there are slow internal motions the apparent coupling constants are the result of motional averaging. We have presented the methodology for structure determination on the basis of a model having two distinct conformers in dynamic equilibrium.[33] The coupling constants, as well as NOE intensities, can be expressed as an average when writing a pseudoenergy function. The psuedoenergy functions for the observed coupling constants interpreted as an average can be expressed as in Eq. (6) simply by calculating coupling constants as a weighted average [Eq. (5)].

$$J = f_1 J_1 + f_2 J_2 \quad (5)$$

$$E_J = W(J - J_0)^2 \quad (6)$$

Here, the J_i are the coupling constants for each conformer and the f_i are the fractional populations of states i. The total energy is the sum of the molecular energy of the two conformers and a pseudoenergy for each observed NOE and coupling constant.

As in our previous work,[4] molecular mechanics calculations were carried out in three steps, using a modified version of AMBER.[34] Starting structures were those generated previously using the first three stages of the DISGEO program[35] and minimizing with an AMBER version modified only to include NOE pseudoenergy functions.[29] Miminization of each structure with both coupling constant pseudoenergies and NOE pseudoenergies was initially carried out using simplified molecular potentials and high pseudoenergy weightings in order to get a potential energy surface with fewer local minima. This step required about 10 hours on a Vax station 3200. Then, all molecular energy terms were added and the structures were minimized further. Finally the structures were relaxed with psuedoenergy functions weighted to allow an equitable balance between violation of molecular energy and NMR constraints (W~729 Å^6 × 30 kcal/mol for the NOE function[36] and 3 kcal/mol/Hz^2 for the coupling constant function). Each of the second and third steps required 2–3 hours computational time on a Multiflow trace 7 computer.

Previous molecular mechanics calculations with NOE pseudoenergies showed reasonable convergence to a single structure despite potential local minimum problems with the approach. In part, this is the result of using a well-behaved pseudoenergy function. The NOE distance pseudoenergy function has a single minimum. Moreover, it allows near neighbor constraints to dominate the energy at each step of the process. We do not anticipate this degree of success with the J pseudoenergy function described above. Therefore, an approach using molecular dynamics and a protocol similar to simulated annealing[19,30,37] was also explored. Starting structures were first minimized with simplified potentials and highly weighted pseudoenergies for 300 cycles, then heated to 1400 K and held there for 1 ps. This step required 30 minutes of cpu time on a Multiflow trace 7 computer. In a second step, all molecular energy terms were added at 1400 K and 2 ps of dynamics were carried out. Then the systems were cooled down by 50 K every 0.04 ps to 300 K and held for 1 ps at 300 K. These steps required 12–20 hours of computational time on Multiflow trace 7 computer depending on the step size of the dynamics calculation. Finally minimizations with low-weight pseudoenergies were carried out to relax the conformations.

RESULTS AND DISCUSSION

Coupling constants (J) and linewidths (ω) extracted from the DQF-COSY data for NH-C_αH protons, are listed in Table 1. V_a *and* V_d are the directly measured separation of extrema in absorption and dispersion spectra. Details of procedures for converting these to coupling constants are given in ref. 18. Only 54 NH-C_αH cross-peaks are tabulated because cross-peaks from the other residues are poorly resolved.

Side chain coupling constants extracted from a P.E.COSY spectrum and the resulting χ values are given in Table II. Figure 2 illustrates extraction of the side chain couplings between α and β protons for Asp-38. It shows an expansion of the α, β region of the P.E.COSY spectrum containing Asp-38 $\alpha\beta_1$ and $\alpha\beta_2$ cross-peaks (a), rows extracted as indicated by dotted lines (b), and a NOESY spectrum of the corresponding NH-α region (c). $J_{\alpha\beta 1}$ and $J_{\alpha\beta 2}$ are measured directly from zero crossing points in the P.E.COSY spectrum as shown in Figure 2b. Note

TABLE I. $^3J_{HN\alpha}$ Coupling Constants for ACP*

Residue	V_a	V_d	J	ω
3	8.9	25.6	3	14
5	8.1	19.4	6	9
6	9.1	25.6	4	14
7	9.7	28.5	4	16
8	9.7	20.9	8	9
10	9.0	24.1	5	13
11	9.7	25.6	6	13
14	9.7	24.4	7	12
15	10.5	24.4	8	12
17	11.4	25.6	10	12
18	8.5	23.3	5	12
19	7.0	17.4	5	9
20	8.1	18.6	7	9
21	10.5	22.5	9	10
22	10.5	25.6	8	13
23	11.0	27.0	8	13
24	8.1	20.0	6	10
26	9.0	20.9	7	10
27	12.0	29.1	9	14
29	10.5	27.9	6	15
30	9.1	23.6	6	12
31	11.2	26.7	9	13
34	8.5	23.3	5	12
35	11.6	29.1	8	15
36	7.7	20.9	5	11
37	9.3	25.6	5	14
38	9.7	27.6	5	15
39	9.0	26.0	4	15
40	8.9	24.7	5	14
41	9.1	24.4	6	13
43	8.7	24.4	5	14
45	9.3	26.7	4	15
46	9.3	23.5	7	12
47	5.8	13.6	5	7
48	8.4	23.8	4	13
49	5.8	14.0	5	7
50	13.4	31.4	11	16
53	10.5	22.1	9	10
54	10.5	29.1	5	16
56	9.3	23.3	7	12
57	7.0	15.1	6	7
58	11.6	27.1	9	13
59	8.1	18.6	7	9
61	10.5	25.6	8	13
63	10.5	26.7	7	14
65	10.5	26.9	9	9
67	10.5	23.3	9	11
68	8.5	24.4	3	13
70	9.3	25.6	5	14
72	10.2	29.1	4	16
73	8.1	22.7	4	12
75	10.5	24.4	8	12
76	9.3	26.7	3	15

*J and ω are in Hz.

that the β_2 coupling is measured from the β_1 cross-peaks and vice versa.

Stereospecific assignment of cross peaks to β_1 and β_2 is done by combining coupling constants, $J_{\alpha\beta1}$ and $J_{\alpha\beta2}$ with the strength of intraresidue NOEs.[38] The patterns of NOEs and J coupling for sterically allowed rotamers are depicted in Figure 3. Clearly the observed pattern is most consistent with rotamer II. Stereospecific assignments are as indicated with β_2 resonating at 2.47 ppm and β_1 resonating at 3.07 ppm. $\chi_{\alpha\beta}$, can be assigned a value of 300°.

Specific assignments such as that described above can be made in the absence of conformational averaging. In the case described the measurement of two values of J, both of which independently give $\chi = 300°$, supports a low level of conformational averaging. The relative intensity of α–β NOEs also would deviate if rotamers were significantly distorted, or conformational averaging occurred. $J_{\alpha\beta1}$ *and* $J_{\alpha\beta2}$ of Gln-19, Ser-27, and Asp-51 in Table II are slightly bigger than 4 Hz which is expected value for $\chi = 60°$. These may result from conformational averaging. χ values for only 12 residues are listed in Table II. Although other coupling constants were measured, only these fit clearly into an ideally rigid model and allowed stereospecific assignment.

We used the 54 $^3J_{HN\alpha}$ coupling constants and 12 χ side chain angles, as well as approximately 450 NOE distance constraints, to refine the 3-D structure of ACP. The pseudoenergy functions described above, were used simultaneously to represent the distance and coupling constant constraints, and starting structures from structures previously identified as B and E were employed.[3] New structures were generated using both molecular dynamics and molecular mechanics protocols.

Table III presents a summary of results coded by method (MM for molecular mechanics and MD for molecular dynamics), data included (D for only distance constraints, C for distance and coupling constant constraints) and, starting structure (B, E, or BE, a two-state model). The first column shows RMS deviation from distance constraints. Note that distance constraints are satisfied well in all cases (<0.6 Å). Coupling constants constraints, however, show large violations (>1.2 Hz, second column in Table III) unless they are explicitly included. Inclusion of coupling constant constraints brings agreement well within experimental error for $J_{HN\alpha}$, while there is little degradation in the RMS distance violation and only moderate increases in molecular energy.

Figure 4a shows Ramachandran plots[39,40] for the backbone torsion angles of structures MMD B and MMC B. The lines beginning at the symbols show the movement from starting structure angles (MMD B) to final structure angles (MMC B) under the influence of both distance and coupling constant constraints using the molecular mechanics protocol. The starting points are plotted in the range from −180° to 180° and the final points are plotted in the range from −270° to 270° to more accurately depict the actual movement. The boxes show the limits of normal right-handed (α_R) and left-handed (α_L) α-helices. The boxes denoted by S include the regions for β sheets, polyglycine II, and collagen.[39,40] Seven residues show large movements of Ψ over 90°. A 90° rotation is very likely to represent movement over rotational barriers. But only two residues show

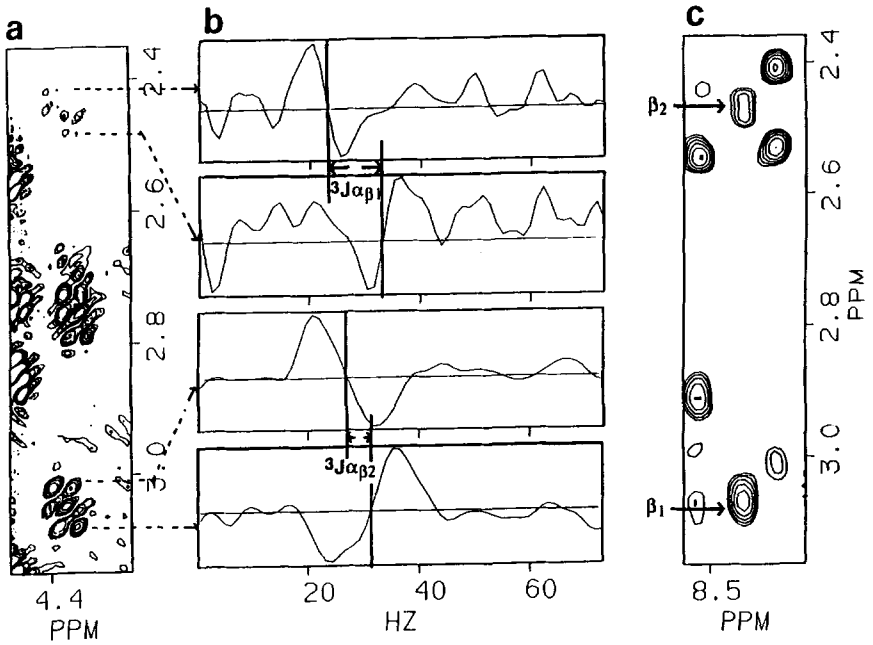

Fig. 2. Data for stereospecific assignment of β protons. Expansion of a P.E.COSY spectrum of ACP showing Asp-38 α–β connectivities (**a**). Rows through cross peaks with digital resolution 1.1 Hz/pt in F_2 (**b**). NOESY spectrum of the NH-C^βH region of Asp-38 (**c**).

TABLE II. Coupling Constants and Side Chain Angles for Stereospecifically Assigned β Protons

Residue	$J_{\alpha\beta1}$ (Hz)	$J_{\alpha\beta2}$ (Hz)	χ (°)
Gln-19	7.3	6.7	60
Asn-24	7.9	4.3	300
Ser-27	6.1	6.1	60
Asp-31	10.8	3.1	300
Asp-35	6.7	4.3	60
Asp-38	11.6	3.1	300
Leu-42	5.5	8.5	180
Asp-51	7.3	6.1	60
Asp-56	9.8	3.1	300
Asn-73	4.9	8.5	180
His-75	9.8	3.7	300
Gln-76	10.4	3.7	300

large movements of Φ over 90°. These are found in loop regions (16–36, 51–65) and the movement probably indicates poor structure definition on the basis of distance constraints only. All the other residues moved to lesser degrees.

The structures were also calculated using the molecular dynamics approach to see if the lack of movement in more structured regions of the protein resulted from local minimum traps. Figure 4b shows a Ramachandran plot at the end of a molecular dynamics cycle with lines showing the movement of points from the MMC B structure to those of the MDC B structure. Six additional residues show a movement of over 90° in Φ and 11 residues show a movement greater than 90° in Ψ. This plot shows a somewhat wider spread of movement in backbone conformation when a molecular dynamics approach is used, and relatively fewer points are now left well outside regions assigned to normal secondary structure. However, as shown in Table III the molecular energy for the MDC B structure is higher than that of the MMC B structure. While the molecular dynamics protocol clearly can overcome some local minimum potential energy barriers, it does not necessarily lead to a better overall structure in a single cycle. A similar protocol was repeated in a search for a better structure. The system was reheated to 1400 K with a low weighted pseudoenergy function and full molecular force fields. It was then held for 1 ps at 1400 K and cooled as described in methods. The energy of this structure was slightly lower (40 kcal/mol) but remained at a significantly higher energy than the MMC B structure.

A combination of deviation from NOE distance observations and high molecular energies had previously led us to propose a two state model for ACP.[33] Structure MMD BE was produced using only distance constraints and this model. Even though the number of coupling constant violations in the one state structures discussed above are small, incorrect interpretation of averaged constants can lead to false minima with high molecular energies. Observed coupling constants were, therefore, reinterpreted as an average and included in the calculation. In analogy with the one-state calculations, the starting structure for MMC BE was MMD BE. The mole fraction 0.5 of each conformation was chosen to optimize fit to experimental NOE and coupling con-

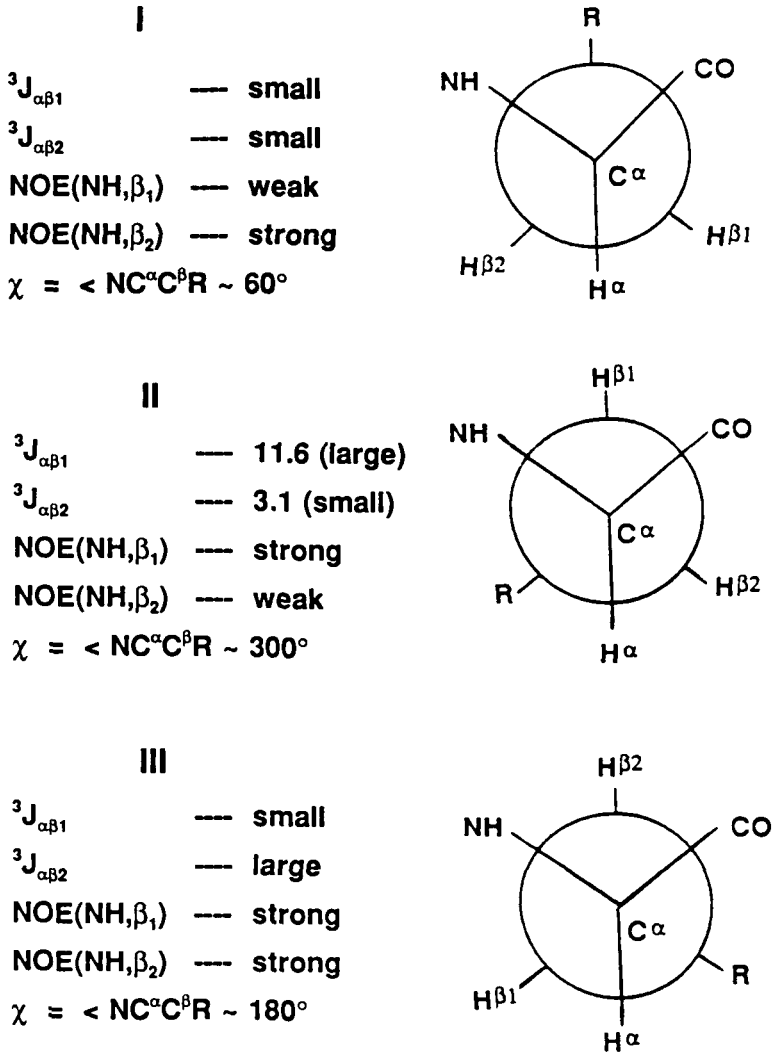

Fig. 3. Rotamer models for interpreting NOEs and *J* coupling constant patterns. Residue 38 is assigned to rotamer II using the data in Figure 2.

TABLE III. Evaluation of the Structures of ACP

Structure	RMS dist. dev. (Å)	RMS $J_{HN\alpha}$ dev. (Hz)	RMS χ dev. (deg)	Molecular energy (kcal/mol)	Number of distance dev. over 2 Å	Number of $J_{HN\alpha}$ dev. over over 1.2 Hz
MMD B*	0.50	2.78	—†	300	6	35
MMD E	0.57	2.89	—	1300	3	40
MMC B	0.50	0.49	12.2	368	2	1
MMC E	0.56	0.65	34.4	1650	4	5
MDC B	0.53	0.56	—	621	5	3
MDC E	0.53	0.69	—	979	4	5
MMD BE	0.28	2.55	—	−190	0	36
MMC BE	0.43	0.56	—	−2	1	2

*The notation for each structure is as follows: The first two letters indicate the calculation method (MM, molecular mechanics or MD molecular dynamics). The third letter indicates a calculation (with just distance constraints, D, or with distance and coupling constant constraints, C). The last letter indicates the starting structure, B, E, or BE.

†Only calculations MMC B and MMC E included minimization with χ angles.

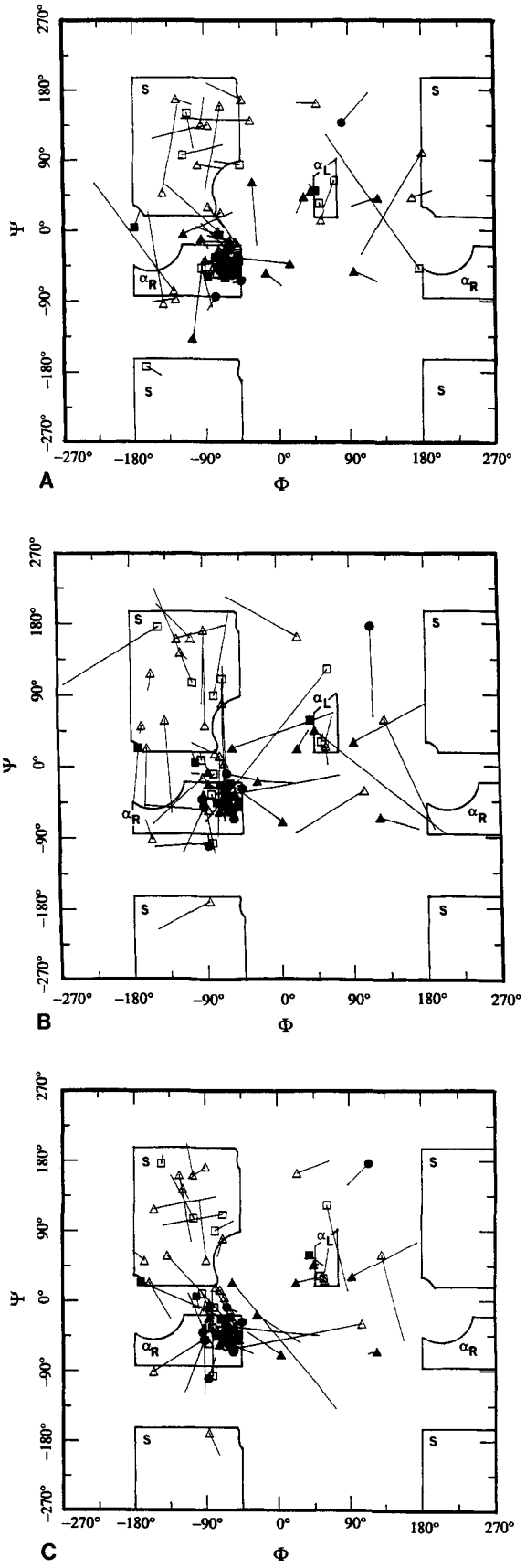

stant data before minimization. Mole fraction 0.5 gives minimization of RMS deviation from distance constraints and RMS deviation from coupling constant constraints. The results are shown in Table III. With a very slight increase of RMS distance deviation and molecular energies over the MMD BE model, the two-state model minimized with coupling constant constraints produces an improved fit to the coupling constant data and a B structure energy much improved over that of MMC B. Figure 4c shows a Ramachandran plot for the B part of the pair of structures with lines showing a movement of points from MMC B to the B structure of MMC BE. Four points show a movement over 90° in Φ and five points show a movement over 90° in Ψ on adding coupling constant constraints. Again the movements are concentrated in the loop regions.

Calculated coupling constants of 27 residues of the B conformer in the two-state model MMC BE are 1 Hz or more away from the observed coupling constant and those of 27 residues of the E conformer in this model are 1 Hz or more away from the observed coupling constant. However, only four residues have average coupling constants lying 1 Hz or more away from the observed coupling constant when the calculated average coupling constant is considered. These four deviations may reflect a failure to find an optimum structure without molecular dynamics cycling. Note in Table III that both long-distance violations and large coupling constant violations decrease significantly on going to the two-state models. The low energy conformer in both two state models MMD BE and MMC BE is energetically much more stable than any conformation of the one state models.

Structures B and E produced by the MMC BE model are depicted in Figure 5. RMS deviation of backbone atoms between those two structures is 4.0 and RMS deviation of all atoms is 5.3, but they continue to show the three helix motif found in previous studies, and should provide useful starting points for discussion of molecular function.

CONCLUSIONS

Addition of coupling constant data has improved our structural description for ACP, especially in loop regions that may not have been constrained enough

Fig. 4. Ramachandran plots for the backbone structure of B. (**A**) The Ramachandran plots for the MMD B structure with the lines showing the movement of each point to its position in the MMC B structure. (**B**) The Ramachandran plots for the MMC B structure with lines showing the movement of each point to its position in the MDC B structure. (**C**) The Ramachandran plots for the MMC B structure with lines showing the movement of each point to its position in the B structure of MMC BE two state model. Each symbol indicates residues in following regions; ▲: first α helix (3–15), ■: second α helix (37–51), ●: third α helix (65–75), △: first loop (16–36), □: second loop (52–64).

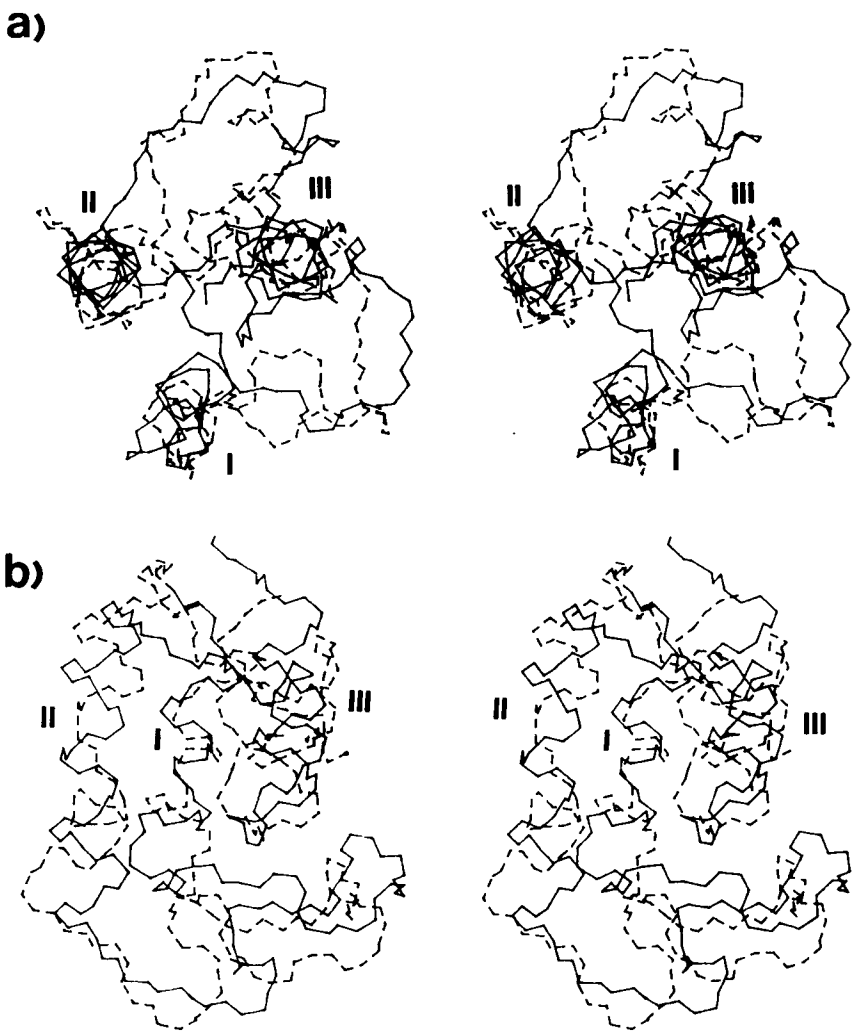

Fig. 5. Stereoviews of the backbone atoms of the two state model MMC BE. (**a**) Compares the end-on alpha-helical views of the backbone structure of B (solid lines) and E (dotted lines). (**b**) The side views of B and E structures in the MMC BE two-state model.

with distance constraints alone. However, inclusion of coupling constant data has not removed the need to use a two-state dynamic averaging model to described the structure of ACP. For one-state solutions, a few molecular dynamics cycles improve local structures by overcoming the local minima associated with the presence of a new J pseudoenergy function, but in terms of overall molecular structure, only the inclusion of a two-state model gives significant improvement in molecular energies. In principle, the best way to approach structure determination for a flexible protein like ACP would be with a method using molecular dynamics protocols along with a two-state model. At present, this approach would be a very computationally demanding process.

ACKNOWLEDGMENTS

This work was supported by a research grant from the National Institutes of Health (GM32243). We thank R. Kriwachi for useful discussions on the P.E.COSY experiment.

REFERENCES

1. Braun, W., Wider, G., Lee, K. H., Wuthrich, K. Conformation of glucagon in a lipid-water interphase by ^{1}H nuclear magnetic resonance. J. Mol. Biol. 169:921–948, 1983.
2. Havel, T. F., Wuthrich, K. An evaluation of the combined use of nuclear magnetic resonance and distance geometry for the determination of protein conformations in solution. J. Mol. Biol. 182:281–294, 1985.
3. Clore G. M., Gronenborn, A. M., Brunger, A. T., Karplus, M. Solution conformation of a Heptadecapeptide comprising the DNA binding helix F of the cyclic AMP receptor protein of *Escherichia coli:* Combined use of ^{1}H nuclear magnetic resonance and restrained molecular dynamics. J. Mol. Biol. 186:435–455, 1985.
4. Holak, T. A., Kearsely, S. K., Kim, Y., Prestegard, J. H. The three-dimensional structure of acyl carrier protein determined by NMR-pseudoenergy and distance geometry calculations. Biochemistry 27:6135–6142, 1988.
5. Kline, A. D., Braun, W., Wuthrich, K. Determination of the complete three-dimensional structure of the α-amylase inhibitor tendamistat in aqueous solution by nuclear mag-

netic resonance and distance geometry. J. Mol. Biol. 204: 675–724, 1988.
6. Moore, J. M., Case, D. A., Chazin, W. J., Gippert, G. P., Havel, T. F., Powls, R., Wright, P. E. Three-dimensional solution structure of plastocyanin from the green alga *Scenedesmus obliquus*. Science 240:314–317, 1988.
7. Karplus, M. Contact electron-spin coupling of nuclear magnetic moments. J. Chem. Phys. 30:11–15, 1959.
8. Ramachandran, G. N., Chandrasekaran, R., Kopple, K. D. Variation of the NH-$C^{\alpha}H$ coupling constant with dihedral angle in the NMR spectra of peptides. Biopolymers 10: 2113–2131, 1971.
9. Bystrov, V. F. Spin-spin coupling and the conformational states of peptide systems. Progr. NMR Spectrosc. 10:41–81, 1976.
10. Pardi, A., Billeter, M., Wuthrich, K. Calibration of the angular dependence of the amide proton-C^{α} proton coupling constants, $^3J_{HN\alpha}$, in a globular protein-use of $^3J_{HN\alpha}$ for identification of helical secondary structure. J. Mol. Biol. 180:741–751, 1984.
11. Clore, G. M., Sukumaran, D. K., Nilges, M., Zarbock, J., Gronenborn, A. M. The conformations of hirudin in solution: A study using nuclear magnetic resonance, distance geometry and restrained molecular dynamics. EMBO J. 6:529–537, 1987.
12. Clore, G. M., Sukumaran, D. K., Nilges, M., Gronenborn, A. M. Three-dimensional structure of phoratoxin in solution: Combined use of nuclear magnetic resonance, distance geometry, and restrained molecular dynamics. Biochemistry 26:1732–1745, 1987.
13. Driscoll, P. C., Clore, G. M., Beress, L., Gronenborn, A. M. A proton nuclear magnetic resonance study of the antihypertensive and antiviral protein BDS-I from the sea anemone *Anemonia sulcata:* Sequential and stereospecific resonance assignment and secondary structure. Biochemistry 28:2178–2187, 1989.
14. Holak, T. A., Nilges, M., Oschkinat, H. Improved strategies for the determination of protein structures from NMR data: The solution structure of acyl carrier proteins. FEBS Lett. 242:218–224, 1989.
15. Neuhaus, D., Wagner, G., Vasak, M., Kagi, J. H. R., Wuthrich, K. Systematic application of high-resolution, phase-sensitive two-dimensional ^{1}H-NMR techniques for the identification of the amino-acid-proton spin systems in proteins-rabbit metallothionein-2. Eur. J. Biochem. 151: 257–273, 1985.
16. Widmer, H., Wuthrich, K. Simulation of two-dimensional NMR experiments using numerical density matrix calculations. J. Magn. Reson. 70:270–279, 1986.
17. Hyberts, S. G., Marki, W., Wagner, G. Stereospecific assignments of side-chain protons and characterization of torsion angles in Eglin C. Eur. J. Biochem. 164:625–635, 1987.
18. Kim, Y., Prestegard, J. H. Measurement of vicinal couplings from cross peaks in COSY spectra. J. Magn. Reson. 84:9–13, 1989.
19. Holak, T. A., Nilges, M., Prestegard, J. H., Gronenborn, A. M., Clore, G. M. Three-dimensional structure of acyl carrier protein in solution determined by nuclear magnetic resonance and the combined use of dynamical simulated annealing and distance geometry. Eur. J. Biochem. 175: 9–15, 1988.
20. Holak, T. A., Prestegard, J. H. Secondary structure of acyl carrier protein as derived from two-dimensional ^{1}H NMR spectroscopy. Biochemistry 25:5766–5774, 1986.
21. Mueller, L. P.E. COSY, a simple alternative to E.COSY. J. Magn. Reson. 72:191–196, 1987.
22. Bax, A., Lerner, L. Measurement of ^{1}H-^{1}H coupling constants in DNA fragments by 2D NMR. J. Magn. Reson. 79:429–438, 1988.
23. Rock, C. O., Cronan, J. E., Jr. Acyl carrier protein from *Escherichia coli*. Methods Enzymol. 71:341–351, 1981.
24. Griesinger, C., Sorensen, O. W., Ernst, R. R. Two-dimensional correlation of connected NMR transitions. J. Am. Chem. Soc. 107:6394–6396, 1985.
25. Griesinger, C., Sorensen, O. W., Ernst, R. R. Practical aspects of the E.COSY technique. Measurement of scalar spin-spin coupling constants in peptides. J. Magn. Reson. 75:474–492, 1987.
26. Bodenhausen, G., Vold, R. L., Vold, R. R. Multiple quantum spin-echo spectroscopy. J. Magn. Reson. 37:93–106, 1980.
27. Redfield, A. G., Kuntz, D. Quadrature fourier NMR detection: Simple multiplex for dual detection and discussion. J. Magn. Reson. 19:250–254, 1975.
28. FTNMR is a program licenced from Hare Research Inc., Woodinville, WA.
29. Scarsdale, J. N., Ram, P., Yu, R. K., Prestegard, J. H. A molecular mechanics-NMR pseudoenergy approach to the solution conformation of glycolipids. J. Comp. Chem. 9: 133–147, 1988.
30. Folkers, P. J. M., Clore, G. M., Driscoll, P. C., Dodt, J., Kohler, S., Gronenborn, A. M. Solution structure of recombinant hirudin and the Lys-47→RGlu mutant: A nuclear magnetic resonance and hybrid distance geometry-dynamical simulated annealing study. Biochemistry 28:2601–2617, 1989.
31. Clore, G. M., Nilges, M., Sukumaran, D. K., Brunger, A. T., Karplus, M., Gronenborn, A. M. The three-dimensional structure of α1-purothionin in solution: Combined use of nuclear magnetic resonance distance geometry and restrained molecular dynamics. EMBO J. 5:2729–2735, 1986.
32. Demarco, A., Llinas, M., Wuthrich, K. Analysis of the ^{1}H-NMR spectra of ferrichrome peptides. I. The non-amide protons. Biopolymers 17:617–636, 1978.
33. Kim, Y., Prestegard, J. H. A dynamic model for the structure of acyl carrier protein in solution. Biochemistry 28: 8792–8797, 1989.
34. Singh, U. C., Weiner, P. K., Case, D. A. Caldwell, J., Kollman, P. A. AMBER 3.0, A program obtained through a licensing agreement with the Reagents of the University of California at San Francisco, 1986.
35. Havel, T. F., DISGEO, Quantum Chemistry Program Exchange. Program No. 507, Indiana University, 1986.
36. Holak, T. A., Forman, J. D., Prestegard, J. H. NMR-pseudoenergy approach to the solution structure of acyl carrier protein. Biochemistry 26:4652–4660, 1987.
37. Clore, G. M., Gronenborn, A. M. Determination of three-dimensional structures of proteins and nucleic acids in solution by nuclear magnetic resonance spectroscopy. CRC Rev. Biochem. Mol. Biol. 24:479–564, 1989.
38. Wagner, G., Braun, W., Havel, T. F., Schaumann, T., Go, N., Wuthrich, K. Protein structures in solution by nuclear magnetic resonance and distance geometry: The polypeptide fold of the basic pancreatic trypsin inhibitor determination using two different algorithms, DISGEO and DISMAN. J. Mol. Biol. 196:611–639, 1987.
39. Ramachandran G. N., Ramakrishnan, C., Sasisekharan, V. Stereochemistry of polypeptide chain configurations. J. Mol. Biol. 7:95–99, 1963.
40. Cantor, C. R., Schimmel, P. R. "Biophysical Chemistry. Part I: The Conformation of Biological Macromolecules" San Francisco: W. H. Freeman, 1980:253–309.